



Chladni Patterns in a Liquid at Microscale

Gaël Vuillemeret

École Polytechnique, Palaiseau 91128, France

Pierre-Yves Gires, Fabrice Casset, and Cédric Poulain*

Université Grenoble Alpes, F-38000 Grenoble, France and CEA LETI MINATEC Campus, F-38054 Grenoble, France

(Received 17 December 2015; revised manuscript received 15 February 2016; published 2 May 2016)

By means of ultrathin silicon membranes excited in the low ultrasound range, we show for the first time that it is possible to form two-dimensional Chladni patterns of microbeads in liquid. Unlike the well-known effect in a gaseous environment at the macroscale, where gravity effects are generally dominant, leading particles towards the nodal regions of displacement, we show that the combined effects of an ultrathin plate excited at low frequency (yielding to subsonic waves) together with reduced gravity (arising from buoyancy) will enhance the importance of microstreaming in the Chladni problem. Here, we report that for micrometric beads larger than the inner streaming layer, the microscale streaming in the vicinity of the plate tends to gather particles in antinodal regions of vibrations yielding to patterns in good agreement with the predicted modes for a liquid-loaded plate. Interestingly, a symmetry breaking phenomenon together with the streaming can trigger movements of beads departing from one cluster to another. We show that, for higher modes, this movement can appear as a collective rotation of the beads in the manner of a “farandole.”

DOI: [10.1103/PhysRevLett.116.184501](https://doi.org/10.1103/PhysRevLett.116.184501)

Recent scientific progress in materials, microelectronics, and biological sciences has made possible the design of a variety of substrates with predetermined patterns that allow the precise positioning of micro- and nanoparticles, or living cells on surfaces. The ability to arrange cells and micro-particles into desired patterns, like microarrays [1], is critical for numerous biological studies and applications such as cell differentiation experiments [2], tissue engineering [3], and multiple cell types coculture [4]. Most existing methods for automated patterning of cells require prefabricated patterns often prepared in clean room conditions (e.g., by photolithography, soft lithography, or printing process [4]), hindering the possibility to change it dynamically over time.

To get better control, versatility, and also to increase both the throughput and speed of the pattern formation, a great effort has been made by means of active methods. In particular, acoustic techniques [5] are now capable of achieving switchable patterns of either nanoparticles [6] or cells, at the ensemble or single levels [7,8]. However, patterns are determined when designing the device because of the narrow resonance of the piezoceramic used for actuation. Indeed, the sound wavelength is chosen to match either the size of the fluid cavity or the interdigitated electrodes used for emission on the substrate, and a given device is in general efficient around only one well-defined resonant frequency.

In 1787, the German physicist Chladni showed that sand grains randomly spread on a metal plate could form a wide variety of patterns upon excitation of the edge with a violin bow, and observed that sand grains grouped along the nodal lines of vibration [9]. The patterns, which vary with different modes of resonance, were called Chladni figures. Interestingly, Chladni also reported that very fine particles

(shavings from his violin bow) moved in the opposite direction to the antinodes, hereafter denoted as inverted patterns. The latter behavior was further studied by Faraday [10], who showed that it was caused by air currents in the vicinity of the plate, now known as acoustic streaming.

In this Letter, we will show for the first time that inverted micro-Chladni figures can be obtained on a microscale thin plate in contact with a liquid, potentially opening the path to new particle handling techniques at microscale. The new method enables us to dynamically control the patterns and clusters formed, together with the possibility to change the beads’ microenvironment by their rotation from one well to another. We believe that this possibility could allow new perspectives in biology for the study of cell-cell and cell-substrate interactions, as well as for low cost and efficient mean for patterning surfaces when making a liquid evaporate.

Experiments have been carried out on polysilicon membranes of radius $a = 800 \mu\text{m}$ and a total thickness $h = 5.9 \mu\text{m}$. The membrane is suspended at the bottom of a $725 \mu\text{m}$ in depth circular hole in a silicon substrate (see Fig. 1). The structure is made of mainly two parts: a passive one which consists in a polysilicon ($4 \mu\text{m}$ thick) and a silicon oxide ($1.9 \mu\text{m}$ thick) multilayer, and the active one which is locally made up of $0.5 \mu\text{m}$ thick lead zirconate titanate deposited and patterned onto the membrane back. Details of the manufacturing can be found elsewhere [11].

In order to supply the cavity with liquid and beads, the silicon chip (containing the piezoelectric membrane cavity) is glued to the back of a commercial microfluidic plastic channel (Ibidi μ -Slide I 0.1 Luer) in which a slotted hole of size $2 \text{ mm} \times 4 \text{ mm}$ has been made to allow the fluid to fill in the cavity. The channel is first filled with ethanol to

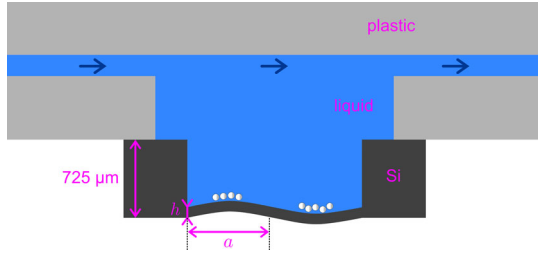


FIG. 1. Sketch of the microfluidic cavity: a silicon chip (containing the membrane) is glued in front of a hole made at the back of a plastic microfluidic channel, allowing liquid supply.

minimize bubble formation, and afterwards with ultrapure water containing microbeads. The microbeads (polystyrene, diameter d between 50 and 70 μm) are visualized by means of reflection microscopy (Zeiss Axioplan II microscope with a $\times 5$ magnification lens and classic halogen illumination). A waveform generator connected to an amplifier is used to drive the piezoelectric membranes. A dc voltage of 15 V is imposed due to the ferroelectric properties of the lead zirconate titanate, in order to ensure the adequate polarization state of the actuator material. An ac voltage, typically 1 V, is then superimposed for dynamic actuation. The vibration amplitude A was obtained from vibrometric analysis (Polytec MSA400) for a nonloaded membrane, assuming a negligible influence of the liquid on the amplitude at the corresponding resonance.

At high frequency ($f > 500$ kHz), the beads do not move and no pattern is observed. When decreasing the sound frequency to the low ultrasound range ($10 < f < 300$ kHz), and for some well-defined frequencies, beads start to move instantaneously at velocities in the range $U \sim 100\text{--}1000 \mu\text{m} \cdot \text{s}^{-1}$ and are attracted towards specific regions on the plate. In fact, as shown in Fig. 2, regular patterns are observed depending on the acoustic frequency. They suggest that beads follow the plate modes of resonance that we are going to predict for a loaded membrane. It is also noteworthy that beads concentrate in antinodal regions of displacement of the plate.

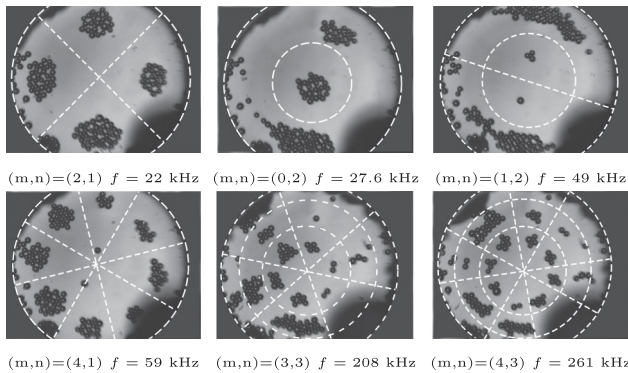


FIG. 2. Top view of the cavity for various frequencies of actuation of the silicon membrane and the corresponding modes (m, n) . The white dashed lines have been plotted to help visualize the nodal lines and circles.

The problem is that of Lamb waves in a bounded domain and has been treated in detail initially by Lamb [12], and further refined [13] (see Supplemental Material [14]). To simplify the treatment, we assume hard-wall conditions as well as the plate to be clamped to it along the circumference. For a nonloaded thin circular plate and looking for time-harmonic solutions, the transverse displacement $w(r, \theta, t) = W(r, \theta) \cos(\omega t)$ obeys the wave equation $(\nabla^4 - k^4)W = 0$, where $k^4 = \rho h(\omega^2/D)$, with $D = [Eh^3/12(1-\nu^2)]$ the flexural rigidity of the plate, E and ν being the Young's modulus and Poisson's ratio, respectively, and $c = \omega/k$ is the velocity of the (antisymmetric) Lamb waves in the plate. Because of the boundary conditions, only discrete eigenmodes exist, each characterized by a doublet (m, n) corresponding, respectively, to the number of its nodal diameters and circles, vibrating at the frequency $f_{m,n}^{\text{unloaded}}$.

For a given (m, n) mode, the effect of water loading can be estimated so that the frequency is reduced to

$$f_{m,n}^{\text{loaded}} = \frac{f_{m,n}^{\text{unloaded}}}{\sqrt{1 + \Gamma_{m,n} \frac{\rho_l a}{\rho_s h}}}, \quad (1)$$

where $\Gamma_{m,n}$ is the nondimensional added virtual mass incremental (NAVMI) factor, which is a generalized version of the AVMI factor initially proposed by Lamb [15]. Values of $\Gamma_{m,n}$ can be found in Ref. [13], Table 5, in the case of a clamped plate. For the first modes of vibration, $\Gamma_{m,n}$ lies in the range 0.05–0.3, so that for our silicon plate in water with $a/h = 130$ the frequency shift will be at least a factor 1/2, confirming the necessity to take loading into account. As shown in Fig. 3, a good agreement is obtained between the predicted values of $f_{m,n}^{\text{loaded}}$ and those observed in our experiment.

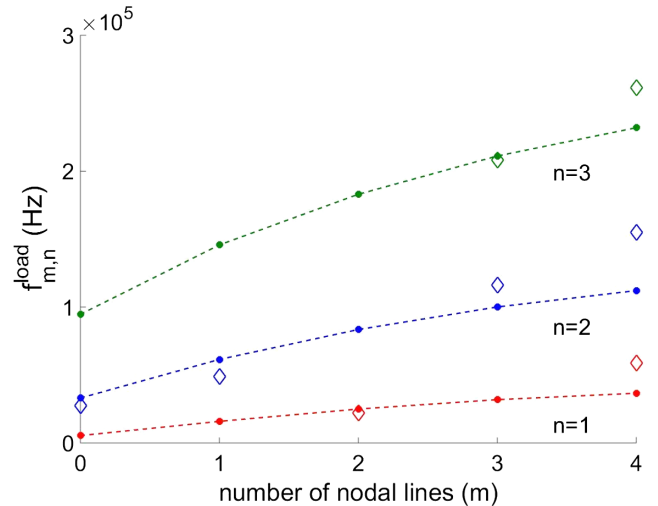


FIG. 3. Mode frequencies $f_{m,n}$ measured (diamond) and calculated (filled circle) by Eq. (1) for a given (m, n) with a circular silicon plate of radius $a = 800 \mu\text{m}$ and thickness $h = 6 \mu\text{m}$. Dotted lines are plotted to guide the reader.

The question of why beads migrate towards the antinodal regions is more subtle and deserves a separate discussion. Recently, different mechanisms have been described which account well for describing inverse Chladni patterns. In particular, Van Gerner has reported and analyzed two distinct mechanisms that could lead to inverse patterns in air. The first one [16] occurs when the plate acceleration is lower than gravity, that is, when a dimensionless number $\Gamma = A\omega^2/g < 1$ (with A the plate amplitude, $\omega = 2\pi f$ the sound pulsation and g the gravitational acceleration). In this case, particles no longer bounce on the plate but rather roll on it and inverse Chladni patterns can be formed without a streaming effect. This approach has to be extended to the general case to take buoyancy into account, when the fluid density is close to the beads' density. Our beads have an excess density $\Delta\rho = \rho_{\text{bead}} - \rho_l = 0.05\rho_l$, and the actual nondimensional Γ in the general case writes $\Gamma = \rho_l A\omega^2/(\Delta\rho g)$. Here, amplitudes of vibration A lie in the range $0.1\text{--}1\ \mu\text{m}$ for the range of frequency $100 > f > 10\ \text{kHz}$ so that in our case, we have $\Gamma \gg 1$; thus the (hysteretic) rolling of beads along the substrate at low acceleration is certainly not at play in our device. In another work [17], Van Gerner shows that when streaming is dominant, and provided that A is large compared with the Stokes layer δ , Lagrangian and Eulerian streaming fields point out in two different directions, explaining the inverse pattern when particles are "light" and driven by the streaming air currents. When particles are "heavy" and gravity dominant, they recover the classical nodal attraction. As $\delta = \sqrt{2\nu/\omega}$, where ν is the liquid kinematic viscosity, we have typically $2 < \delta < 6\ \mu\text{m}$ for corresponding frequencies in the range $100 > f > 10\ \text{kHz}$. We have $A/\delta \ll 1$ so that as they explain in their work, we recover here a more classic picture with Eulerian and Lagrangian fields pointing in the same direction. For the 1D case (vibrations of a cantilever beam in liquid) and provided that $A/\delta \ll 1$, Dorrestijn has shown [18] that the whole streaming velocity profile has to be determined in respect of the bead size d to account for nodal or antinodal migration of beads or nanoparticles, respectively. They give a simple model to emphasize the role of the actual (Eulerian) streaming velocity profile for the micro- or nanobeads' regions of attraction on the cantilever beam.

To compare the relative importance of drag force with respect to gravity, one can estimate the factor $B = (F_{\text{drag}}/F_{\text{gravity}})$ as in Ref. [17] in the case of air. In liquids, buoyancy effects cannot be neglected, so that $B = [3\pi\rho_l\nu d(u-v)/(1/6\pi\Delta\rho g d^3)]$, with u and v the bead and fluid velocity, respectively. Considering microbeads as perfect Lagrangian tracers, we have $u \approx u_s$, where u_s is the typical streaming velocity. To get a rough estimation for the order of magnitude of the streaming velocity, we can use Rayleigh's scaling for the viscous streaming velocity above a vibrating plate, which writes $u_s \sim A^2\omega^2/c$ [19]. Given that

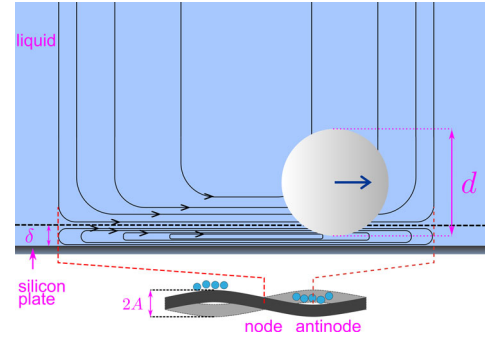


FIG. 4. Sketch of a bead within the inner and outer streaming rolls in our case ($A < \delta < a$): the bead follows the outer streaming direction towards antinodes of vibration of the plate.

$c \propto \sqrt{\omega h}$ and the thickness of the plate, we find $30 < c < 95\ \text{m s}^{-1}$ for the range $10 < f < 100\ \text{kHz}$. It is noteworthy that, since the Lamb waves are always slower than acoustic bulk waves in the liquid ($c_{\text{water}} \approx 1500\ \text{m s}^{-1}$), we are in the subsonic regime in which evanescent waves are generated. Finally, we obtain $40 < u_s < 130\ \mu\text{m s}^{-1}$ for the order of magnitude of the streaming velocity for the aforementioned range of frequencies. This calculated range is between 2 and 10 times smaller than the velocities estimated from image processing of the beads' movement. We think that some approximations, such as considering the multilayered and loaded membrane as nonloaded and homogeneous, lead to an overestimation of the surface waves celerity and hence an underestimation of the streaming velocity.

Using the streaming velocity and assuming that A decreases linearly from $1\ \mu\text{m}$ to $100\ \text{nm}$ when the excitation frequency goes from 10 to $100\ \text{kHz}$, we obtain $3 < B < 10$, confirming that streaming plays a major role in our experiments. Given that streaming is dominant and following Dorrestijn's approach, we expect beads to move towards the regions where the streaming velocity profile integrated over the bead surface points out. In our case, since beads are much larger than the inner streaming layer (i.e., $d \gg \delta$), beads are going to follow the outer streaming direction which is sketched in Fig. 4, extrapolated from

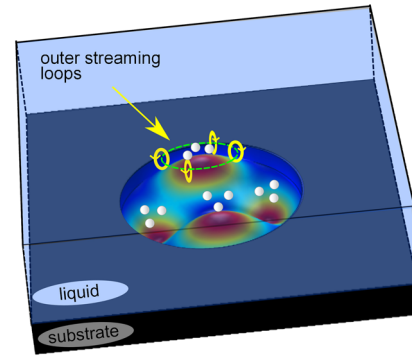


FIG. 5. Schematic view of the trapped beads within the outer streaming loops, for a (2,1) mode. The membrane amplitude, bead, and loop sizes have been magnified for sake of clarity.

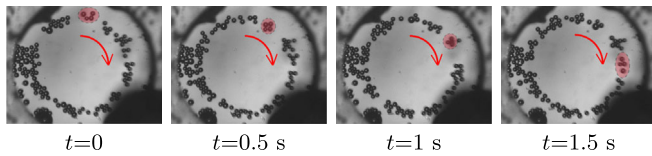


FIG. 6. $70\ \mu\text{m}$ beads in the cavity rotating in a farandolelike manner at $f = 61\ \text{kHz}$. The corresponding stable mode (4,1) is obtained at $59\ \text{kHz}$. The time frame between each picture is $0.5\ \text{s}$.

Dorrestijn’s paper [18] to our case $A \ll \delta \ll d$. As explained in this work, microbeads are carried by the streaming flow towards the plate antinodal regions of vibration, leading to the so-called inverse Chladni patterns. In Fig. 5, we have drawn a 3D schematic picture for the mode $(m, n) = (2, 1)$ to render the beads clusters at the vibration antinodes and the corresponding streaming loops.

As long as the forcing frequency remains the same, the clusters form stable patterns; the beads appear to be frozen at the bottom of the microcavity. However, when slightly shifting the sound frequency (typically 2–3 kHz above a resonant frequency), we observe beads movements, all in the same orthoradial direction, from one cluster of beads to the nearest one. Provided that the initial trapping mode m is high enough (typ. $m > 3$), the global movement appears like a global rotation of the beads, in the manner of a “farandole” dance, either clockwise or anticlockwise depending on the mode chosen.

We have implemented a tracking software (TrackMate from ImageJ) in order to get the movement’s features at any time and position. Figure 6 shows snapshots of the farandole regime obtained for the (4; 1) mode at $f = 61\ \text{kHz}$, Fig. 7(a) displaying the averaged (over time) image obtained in this case. The time-averaged trajectory colored by the orthoradial velocity magnitude v_Ω has been overlaid. It outlines that beads are trapped in the wells until they escape, so that on average they spend more time in the wells than in between them (see also Supplemental Material [14]). Figure 7(b) shows the mean velocity v_Ω for an increasing voltage on the piezoceramic. For every

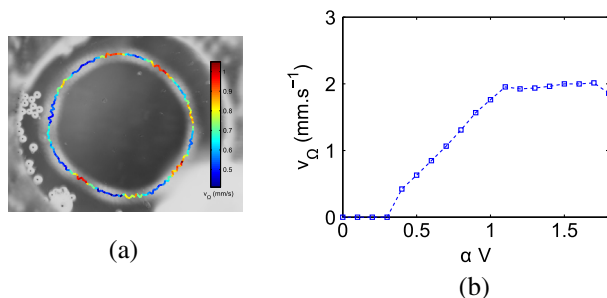


FIG. 7. (a) Averaged (over time) picture of the sequence of frames also used for Fig. 6 on which the mean beads trajectory colored by velocity magnitude is overlaid. (b) Mean orthoradial velocity v_Ω as a function of the applied voltage, at $61\ \text{kHz}$. V is the input voltage and α the amplifier gain, a constant about 1.

experiment, we have observed a threshold below which particles do not move, and a saturationlike behavior of the angular velocity at highest voltages.

As for a complete explanation of the rotation mechanism, we have no clear explanation so far but we can make remarks linked with our observation. First, in the case of a circular membrane, conversely to the case of a square one, for instance, all the nodal lines are equiprobable. In other words, if no symmetry breaking existed, there would be, for a given frequency, no preferred orientation compared with another one (modes are degenerate). Of course, we know that the fabrication process of the membrane yields some residual stress which must lead to a more probable orientation of a given mode of deformation of the plate. When the frequency is shifted, however, it is possible that some modes are close enough in space so that they play the role of a close attractor, triggering bead movement to the nearest trap. Indeed, we observe that if one bead jumps from one trap to another, it seems to trigger an instability for the destination cluster. This trap will in turn release a bead in the same direction, in the manner of a Newton’s cradle (see video in the Supplemental Material [14]) Obviously, this stable feature would not exist in the one-dimensional case of a thin vibrating beam.

In this Letter, we have shown that it is possible to form Chladni patterns at microscale in a liquid by taking advantage of buoyancy in liquid media, thus lowering the effects of gravity, while promoting the importance of streaming near the vibrating wall. We believe that Chladni patterns have never been reported so far in liquids because of the many conditions required for this streaming to be fulfilled. Indeed, since $u_s \sim A^2 f^{1.5}$, use of high frequency could be expected to increase the streaming amplitude. Actually, this dependence is very weak and leads with thick plates to supersonic (fast) waves decreasing the streaming amplitude together with the boundary layer thickness, thus preventing micrometric particles to move. Here, use of an ultrathin silicon plate leads to ultraslow (subsonic) waves enhancing the streaming amplitude in a region comparable with the beads’ size. We believe this strategy could be advantageously extended to other thin substrate and low-cost material for getting a very simple, efficient lab-on-a-chip mean for dynamic patterning of cells or bacteria on a thin substrate for different problems where the control of the local microenvironment is critical.

*cedric.poulain@cea.fr

- [1] C. Flaim, S. Chien, and S. Bhatia, *Nat. Methods* **2**, 119 (2005).
- [2] A. Tourovskaia, X. Figueroa-Masot, and A. Folch, *Lab Chip* **5**, 14 (2005).
- [3] M. M. Stevens, M. Mayer, D. G. Anderson, D. B. Weibel, G. M. Whitesides, and R. Langer, *Biomaterials* **26**, 7636 (2005).

- [4] C. A. Goubko and X. Cao, *Mater. Sci. Eng., C* **29**, 1855 (2009).
- [5] G.-J. Peter and H. Martyn, *Lab Chip* **13**, 1010 (2013).
- [6] B. Raeymaekers, C. Pantea, and D. N. Sinha, *J. Appl. Phys. Lett.* **109**, 014317 (2011).
- [7] D. J. Collins, B. Morahan, J. Garcia-Bustos, C. Doerig, M. Plebanski, and A. Neild, *Nat. Commun.* **6** (2015).
- [8] S. B. Q. Tran, P. Marmottant, and P. Thibault, *Appl. Phys. Lett.* **101**, 114103 (2012).
- [9] E. Chladni, *Entdeckungen ber die Theory des Klanges* (Weidmanns Erben und Reich, Leipzig, 1787).
- [10] M. Faraday, *Phil. Trans. R. Soc. London* **121**, 299 (1831).
- [11] F. Casset, R. Dejaeger, B. Laroche, B. Desloges, Q. Leclere, R. Morisson, Y. Bohard, J. Goglio, J. Escato, and S. Fanget, *Procedia Eng.* **120**, 49 (2015); eurosensors 2015.
- [12] H. Lamb, *Proc. R. Soc. A* **93**, 114 (1917).
- [13] M. Amabili and M. Kwak, *J. Fluids Struct.* **10**, 743 (1996).
- [14] See Supplemental Material at <http://link.aps.org/supplemental/10.1103/PhysRevLett.116.184501> for the theoretical treatment of the resonance of liquid loaded membranes. A processed movie of tracked particles in the farandole regime, with a graph on the particle speed distribution, is also provided.
- [15] H. Lamb, *Proc. R. Soc. A* **98**, 205 (1920).
- [16] H. J. Van Gerner, M. A. van der Hoef, D. Van Der Meer, and K. Van Der Weele, *Phys. Rev. E* **82**, 012301 (2010).
- [17] H. J. van Gerner, K. van der Weele, M. A. van der Hoef, and D. van der Meer, *J. Fluid Mech.* **689**, 203 (2011).
- [18] M. Dorrestijn, A. Bietsch, T. Açıklım, A. Raman, M. Hegner, E. Meyer, and C. Gerber, *Phys. Rev. Lett.* **98**, 026102 (2007).
- [19] L. Rayleigh, *Phil. Trans. R. Soc. London* **175**, 1 (1884).